Effects of attitude constraints on solar sail optimal interplanetary trajectories

Andrea Caruso*, Lorenzo Niccolai, Alessandro A. Quarta, Giovanni Mengali

Department of Civil and Industrial Engineering, University of Pisa, I-56122 Pisa, Italy

Abstract

The aim of this paper is to evaluate the effect of a maximum admissible value of the sail cone angle on the transfer performance of a solar sail-based spacecraft in an interplanetary mission scenario. The proposed approach models the possible constraint on the maximum Sun angle of the solar panels, when thin film solar cells are attached to the flat solar sail exposed area. In particular, transfers towards Mars and Venus are investigated in a simplified circle-to-circle, two-dimensional mission scenario. This study is carried out by analyzing the transfer problem in a systematic way, by considering both the sail characteristic acceleration and the Sun angle of the solar panels as the independent parameters that define the mission performance in terms of flight time.

Keywords: Solar sail, thrust vector constraint, trajectory optimization, interplanetary transfer

Nomenclature

$\boldsymbol{a}$	=	propulsive acceleration vector, $[\mathrm{mm/s^2}]$
a_c	=	characteristic acceleration, $[\mathrm{mm/s^2}]$
a_r	=	radial propulsive acceleration, $[\mathrm{mm/s^2}]$
a_t	=	transverse propulsive acceleration, $[\mathrm{mm/s^2}]$
$\boldsymbol{h}$	=	angular momentum vector, $[\mathrm{au^2/TU_\odot}]$
$\{\hat{\boldsymbol{i}}, \hat{\boldsymbol{j}}, \hat{\boldsymbol{k}}\}$	=	unit vectors along $\{x, y, z\}$
$\{\hat{\boldsymbol{i}}_O, \hat{\boldsymbol{j}}_O, \hat{\boldsymbol{k}}_O\}$	=	unit vectors along $\{x_O, y_O, z_O\}$
$\hat{\boldsymbol{n}}$	=	outward unit vector normal to the sail plane
O	=	Sun's center-of-mass
$\boldsymbol{r}$	=	position vector, $[\mathrm{au}]$
$\hat{\boldsymbol{r}}$	=	radial unit vector
r	=	Sun-spacecraft distance, $[\mathrm{au}]$
$r_\oplus$	=	radius of Earth's heliocentric orbit, $[\mathrm{au}]$
$r_\mars$	=	radius of Mars' heliocentric orbit, $[\mathrm{au}]$
$r_\venus$	=	radius of Venus' heliocentric orbit, $[\mathrm{au}]$
S	=	spacecraft center-of-mass
$\mathcal{T}(O; x, y, z)$	=	heliocentric-ecliptic reference frame
$\mathcal{T}_O(S; x_O, y_O, z_O)$	=	radial-tangential-normal reference frame
$\hat{\boldsymbol{t}}$	=	transverse unit vector
t	=	time, $[\mathrm{days}]$
$\boldsymbol{v}$	=	velocity vector, $[\mathrm{au/TU_\odot^2}]$

*Corresponding author

Email addresses: `andrea.caruso@ing.unipi.it` (Andrea Caruso), `lorenzo.niccolai@ing.unipi.it` (Lorenzo Niccolai), `a.quarta@ing.unipi.it` (Alessandro A. Quarta), `g.mengali@ing.unipi.it` (Giovanni Mengali)

u	=	radial component of the spacecraft velocity, [km/s]
v	=	transverse component of the spacecraft velocity, [km/s]
α	=	cone angle, [deg]
α_a	=	auxiliary control angle, [deg]
$\alpha_a^{\max}$	=	maximum value of α_a, [deg]
Δt	=	constrained minimum fight time, [days]
Δt_u	=	unconstrained minimum fight time, [days]
δ	=	clock angle, [deg]
φ	=	Sun angle of the solar panels, [deg]
$\varphi_{\max}$	=	maximum value of φ, [deg]

1. Introduction

Solar sailing is a fascinating form of propulsion concept that differs from other kinds of systems typically used to generate the thrust necessary to accomplish a given space mission [1, 2]. The distinguishing feature that makes this propulsive form unique is that its thrust is not produced by ejecting propellant from the spacecraft, but exploiting the momentum exchange between a large reflective membrane and the solar photons [3]. Because it uses an unlimited source of energy (the Sun), a solar sail-based spacecraft can theoretically be propelled indefinitely and with continuity, the only limit being the service life of the sail reflective material [4, 5, 6].

Solar sails enable a number of advanced space missions that would be difficult to carry out with traditional propulsion systems [7, 8, 9, 10], such as mission to Kuiper Belt objects [11], multi-asteroid rendezvous [12], asteroid de-spin and deflection [13], debris removal from geostationary orbit [14] . A typical reference mission that is often used to quantify the performance of a solar sail-based spacecraft is an orbit-to-orbit (that is, ephemeris-free), interplanetary transfer towards inner planets [15, 16, 17]. In that case, the transfer is usually studied assuming the spacecraft to be subjected only to the gravitational attraction of the Sun and to the propulsive acceleration provided by the solar sail. In particular, the transfer trajectory is conveniently analyzed within an optimal framework, by looking for the control law that minimizes the flight time required to transfer the vehicle from the Earth's heliocentric orbit to that of the target planet [18, 19, 20]. This amounts to calculating the time histories of the cone and the clock angles that define the orientation of the sail thrust vector with respect to an orbital reference frame [21]. These two control angles may range within an interval that models the physical constraint on the thrust vector direction [22], which cannot be oriented such as to point towards the Sun.

Actually, the whole spacecraft (and so the solar sail) attitude must also take into account other factors such as, for example, the angle of incidence of the sunlight, which may influence the generation of the electric power (through photovoltaic panels that may cover a portion of the sail total area), the vehicle thermal control [23, 24], and the efficiency of the thrust generation caused by the reduced area exposed to solar radiation pressure. Moreover, when considering solar sails with large surface area, substantial attitude variations may be challenging to obtain due to the spacecraft large moment of inertia, and a failure in the attitude control system may prevent certain attitude change maneuvers from being performed during (a part of) the transfer phase. These considerations reduce, in practice, the admissible range of variation of the sail cone angle.

The aim of this work is to model, with a simplified mathematical approach, these additional constraints on the direction of the thrust vector and to investigate optimal solar sail trajectories with reduced admissible range of the sail cone angle. Such a problem was first faced by He et al. [25], who studied a classical Earth-Mars interplanetary transfer, and a transfer from Earth to Asteroid 68278, considering three possible values of the maximum admissible sail cone angle. Their work [25] also reported the optimal control law, and the optimization problem was solved using an indirect approach. Starting from the results described in Ref. [25], this paper provides a systematic analysis for quantifying the impact of the sail cone angle constraints on both the thrust direction and the transfer performance of an orbit-to-orbit interplanetary mission. In particular, transfers towards Mars and Venus are investigated in a simplified (that is, circle-to-circle and two-dimensional) mission scenario [26, 27]. This study is carried out by considering both the solar sail characteristic acceleration and the Sun angle of the solar panels as the independent parameters that define

the transfer performance in terms of flight time. This work also highlights some interesting features, such as the conditions (in terms of characteristic acceleration and maximum Sun angle) for which the constraint on the maximum admissible value of the cone angle is inactive, and, therefore, the results of the constrained and unconstrained transfer problems coincide.

The paper is organized as follows. The next section illustrates the mathematical model that describes the propulsive acceleration vector of an ideal solar sail and the additional constraint on the control angle. Section 3 reports the numerical results, whereas the final section draws the conclusions of this work.

2. Mathematical Model

Consider a solar sail-based spacecraft S, and introduce a heliocentric-ecliptic inertial reference frame $\mathcal{T}(O; x, y, z)$ of unit vectors $\{\hat{\boldsymbol{i}}, \hat{\boldsymbol{j}}, \hat{\boldsymbol{k}}\}$, in which the origin coincides with the Sun's center-of-mass O, the x-axis points towards the vernal equinox, and the z-axis points towards the north ecliptic pole; see Fig. 1, where $\boldsymbol{r}$ (or $\hat{\boldsymbol{r}}$) is the spacecraft position vector (or unit vector).

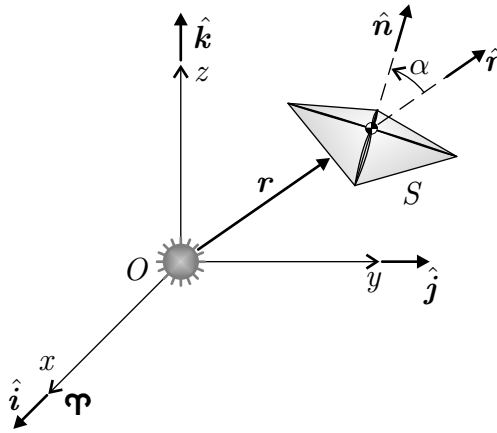

Figure 1: Inertial reference frame $\mathcal{T}(O; x, y, z)$ and sail cone angle α.

In a preliminary and simplified mission analysis, a flat sail and an ideal force model [3] may be assumed, so that the solar sail is approximated as a rigid mirror that specularly reflects all the incident light. A succeeding and more refined analysis, which includes the real thermo-optical characteristics of the reflective film material [21], or the sail billowing [28, 29, 30], represents a straightforward problem. The spacecraft propulsive acceleration vector $\boldsymbol{a}$ is written as [21]

$$\boldsymbol{a} = a_c \left(\frac{r_{\oplus}}{r}\right)^2 \cos^2 \alpha \, \hat{\boldsymbol{n}} \tag{1}$$

where r is the Sun-spacecraft distance (with $r_{\oplus} \triangleq 1 \, \mathrm{au}$), $\hat{\boldsymbol{n}}$ is the unit vector normal to the sail nominal plane in the direction opposite to the Sun, and $\alpha \in [0, 90] \, \deg$ is the sail cone angle, that is, the angle between the Sun-spacecraft line and the direction of $\hat{\boldsymbol{n}}$; see Fig. 1. A sail cone angle $\alpha = 0$ (or $\alpha = 90 \, \deg$) corresponds to a solar sail whose nominal plane is perpendicular (or parallel) to the incident light. In particular, $\alpha = 90 \, \deg$ is the only value of the sail cone angle that allows the propulsive acceleration to be set to zero, such as to introduce a coasting arc in the transfer trajectory. In Eq. (1), a_c is the spacecraft characteristic acceleration, defined as the maximum propulsive acceleration magnitude $\|\boldsymbol{a}\|$ at a reference Sun-sail distance of 1 au. The characteristic acceleration is a typical performance parameter and its value depends on the solar sail design characteristics (such as its side length or the reflective film areal density), and the spacecraft mass budget (payload and mass of the subsystems).

The sail attitude, as well as the components of $\boldsymbol{a}$, are conveniently described by introducing a radial-tangential-normal orbital reference frame $\mathcal{T}_O(S; x_O, y_O, z_O)$ of unit vectors $\{\hat{\boldsymbol{i}}_O, \hat{\boldsymbol{j}}_O, \hat{\boldsymbol{k}}_O\}$. The origin S co-incides with the spacecraft center-of-mass, the z_O-axis is along the Sun-spacecraft line, while the y_O-axis is

3

directed along the spacecraft specific angular momentum vector $\boldsymbol{h} \triangleq \boldsymbol{r} \times \boldsymbol{v}$, where $\boldsymbol{v}$ is the spacecraft inertial velocity; see Fig. 2(a). More precisely, the unit vectors $\{\hat{\boldsymbol{i}}_O, \hat{\boldsymbol{j}}_O, \hat{\boldsymbol{k}}_O\}$ are defined as

$$\hat{\boldsymbol{k}}_O = \hat{\boldsymbol{r}} \triangleq \boldsymbol{r}/r \quad , \qquad \hat{\boldsymbol{j}}_O = \frac{\hat{\boldsymbol{r}} \times \hat{\boldsymbol{v}}}{\|\hat{\boldsymbol{r}} \times \hat{\boldsymbol{v}}\|} \quad , \qquad \hat{\boldsymbol{i}}_O = \hat{\boldsymbol{j}}_O \times \hat{\boldsymbol{k}}_O \tag{2}$$

Note that y_O is undefined when $\hat{\boldsymbol{r}} \times \hat{\boldsymbol{v}} = 0$, that is, when the spacecraft covers a rectilinear orbit [31, 32, 33, 34] which is therefore excluded from the analysis. With the aid of Fig. 2(b), the components of the sail normal

(a) Orbital reference frame.

(b) Sail attitude angles.
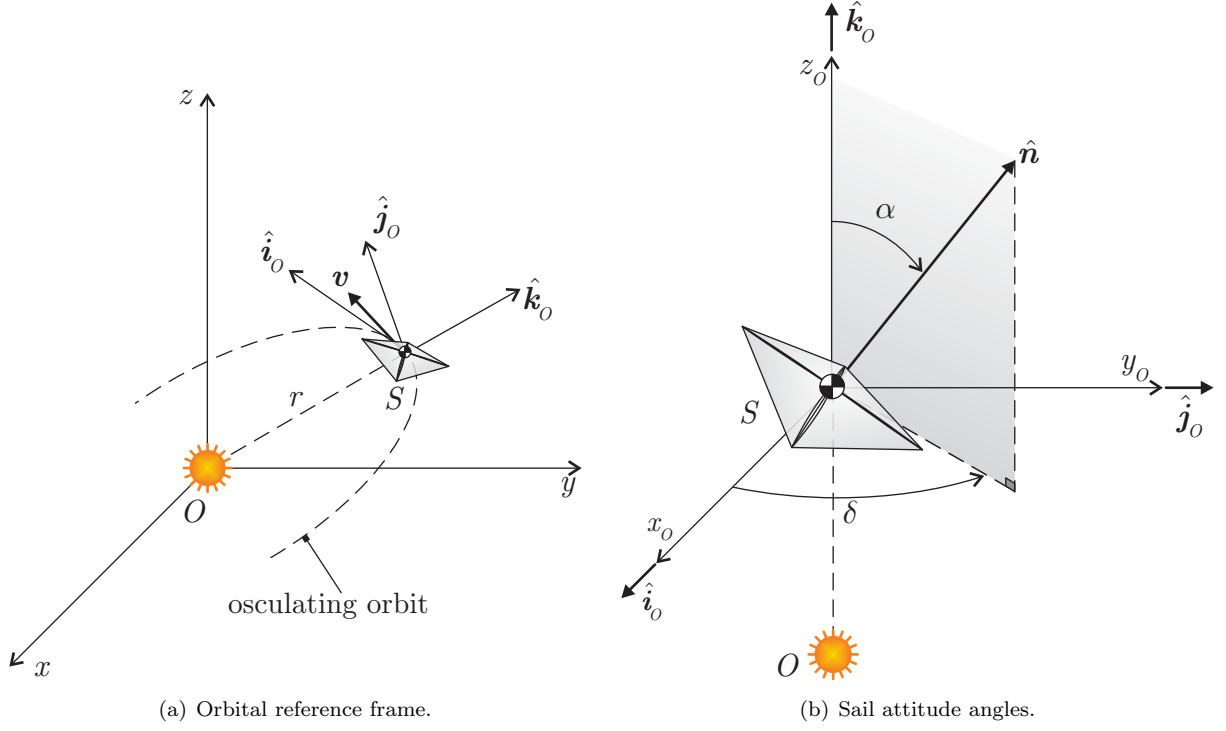
Figure 2: Orbital reference frame $\mathcal{T}_O(S; x_O, y_O, z_O)$ and sail attitude angles $\{\alpha, \delta\}$.

unit vector $\hat{\boldsymbol{n}}$ in $\mathcal{T}_O$ can be written as a function of the cone angle α and the clock angle $\delta \in [0, 360)$ deg, defined as the angle measured counterclockwise from the x_O-axis to the projection of $\hat{\boldsymbol{n}}$ on the (x_O, y_O) plane, viz.

$$\hat{\boldsymbol{n}} = \sin\alpha \, \cos\delta \, \hat{\boldsymbol{i}}_O + \sin\alpha \, \sin\delta \, \hat{\boldsymbol{j}}_O + \cos\alpha \, \hat{\boldsymbol{k}}_O \tag{3}$$

The components of the propulsive acceleration vector may be written in the orbital reference frame by substituting Eq. (3) into Eq. (1). The result is

$$\boldsymbol{a} = a_c \left(\frac{r_\oplus}{r}\right)^2 \cos^2\alpha \, \left(\sin\alpha \, \cos\delta \, \hat{\boldsymbol{i}}_O + \sin\alpha \, \sin\delta \, \hat{\boldsymbol{j}}_O + \cos\alpha \, \hat{\boldsymbol{k}}_O\right) \tag{4}$$

The propulsive acceleration vector can also be conveniently expressed in terms of radial (that is, along the Sun-spacecraft line) and transverse acceleration as

$$\boldsymbol{a} = a_r \, \hat{\boldsymbol{r}} + a_t \, \hat{\boldsymbol{t}} \tag{5}$$

where a_r (or a_t) is the radial (or transverse) component of the propulsive acceleration, that is

$$a_r \triangleq a_c \left(\frac{r_\oplus}{r}\right)^2 \cos^3\alpha \tag{6}$$

$$a_t \triangleq a_c \left(\frac{r_\oplus}{r}\right)^2 \cos^2\alpha \, \sin\alpha \tag{7}$$

4

while $\hat{\boldsymbol{t}}$ is the transverse unit vector [21] defined as

$$\hat{\boldsymbol{t}} \triangleq \cos\delta\,\hat{\boldsymbol{i}}_O + \sin\delta\,\hat{\boldsymbol{j}}_O \tag{8}$$

The function $a_r = a_r(a_t)$ is drawn in Fig. 3, which shows the so-called "force bubble" of the ideal solar sail [35].
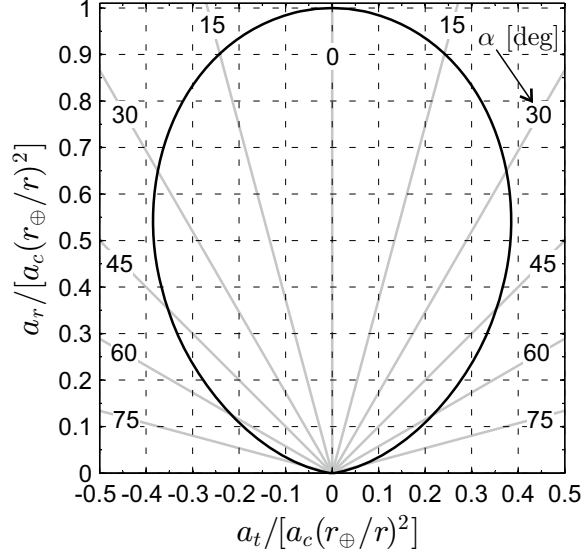

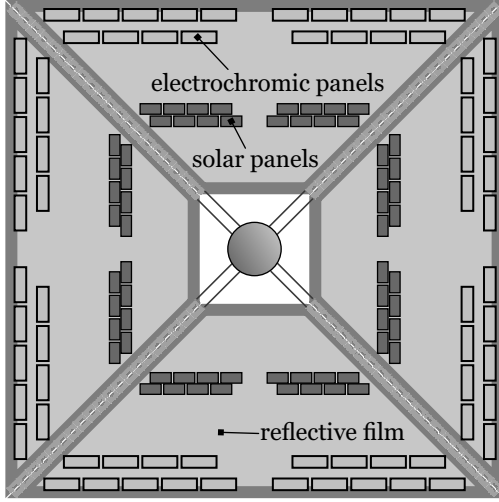Figure 3: Shape of the ideal sail force bubble.

Usually, the solar sail trajectory is the result of a suitable time-variation of both cone and clock angles, obtained as the solution of an optimization problem in which the flight time is the performance index to be minimized. With such an approach to trajectory analysis, the two attitude angles are found with the only constraint that the sail thrust vector (i.e., the normal unit vector $\hat{\boldsymbol{n}}$, see Eq. (1)) is to be oriented away from the Sun. In mathematical terms, this constraint can be written as $\alpha \le 90\,\mathrm{deg}$, which imposes an upper limit on the sail cone angle. In addition, the solar sail thrust may be freely set to zero by orienting $\hat{\boldsymbol{n}}$ orthogonal to the Sun-sail line, that is, by selecting $\alpha = 90\,\mathrm{deg}$. However, when thin film solar cells are attached to the sail exposed area, as in the demonstrator spacecraft IKAROS [23], see Fig. 4(a), a high value of α implies a high value of φ, the latter being the Sun angle of the solar panels; see Fig. 4(b). As a result, a high value of α is likely to decrease the electric power level of a subsystem based on solar arrays. In that case, an upper limit on the maximum value of φ, in the form $\varphi_{\max} \triangleq \max(\varphi) < 90\,\mathrm{deg}$, should be considered during the analysis and optimization of the spacecraft transfer trajectory.

Because the ideal sail is approximated with a flat and rigid reflecting surface, the Sun angle of the solar panels coincides with the sail cone angle, that is, $\varphi \equiv \alpha$. The additional constraint $\varphi \le \varphi_{\max}$ can be therefore rewritten in terms of control angles as

$$\alpha \in [0,\,\varphi_{\max}] \qquad \text{with} \qquad \varphi_{\max} < 90\,\mathrm{deg} \tag{9}$$

in which $\varphi_{\max}$ can be considered as a given parameter that depends on the minimum acceptable level of the electric power. As a consequence of Eq. (9), an ideal solar sail cannot set the propulsive acceleration magnitude to zero, that is, coasting arcs are forbidden during the transfer. From a geometrical point of view, the effect of the presence of $\varphi_{\max}$ on the solar sail thrust vector can be appreciated in Fig. 5, which shows the constrained ideal sail force bubble for $\varphi_{\max} = \{30, 60\}\,\mathrm{deg}$. In particular, the shaded area of Fig. 5 gives the pairs $\{a_r, a_t\}$ for which $\varphi > \varphi_{\max}$. Note that, according to Fig. 5, for a given value of r, the characteristic acceleration a_c defines the size of the sail force bubble, whereas the value of $\varphi_{\max}$ gives its actual shape.

In other terms, taking into account Eq. (4), the propulsive acceleration vector $\boldsymbol{a}$ at a given Sun-spacecraft distance r is a function of the two control angles $\{\alpha, \delta\}$ and the two design parameters $\{a_c, \varphi_{\max}\}$, where

(a) IKAROS spacecraft. Adapted from Ref. [36].
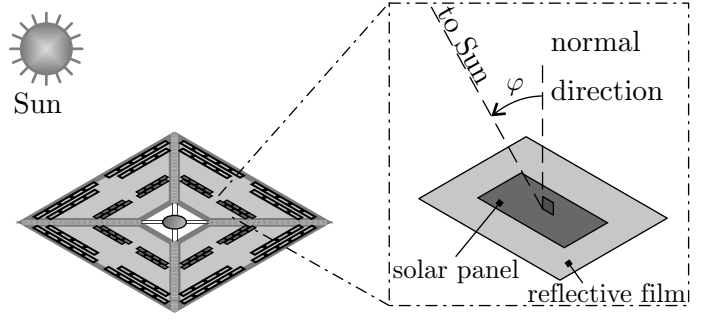
(b) Sun angle of solar panels.

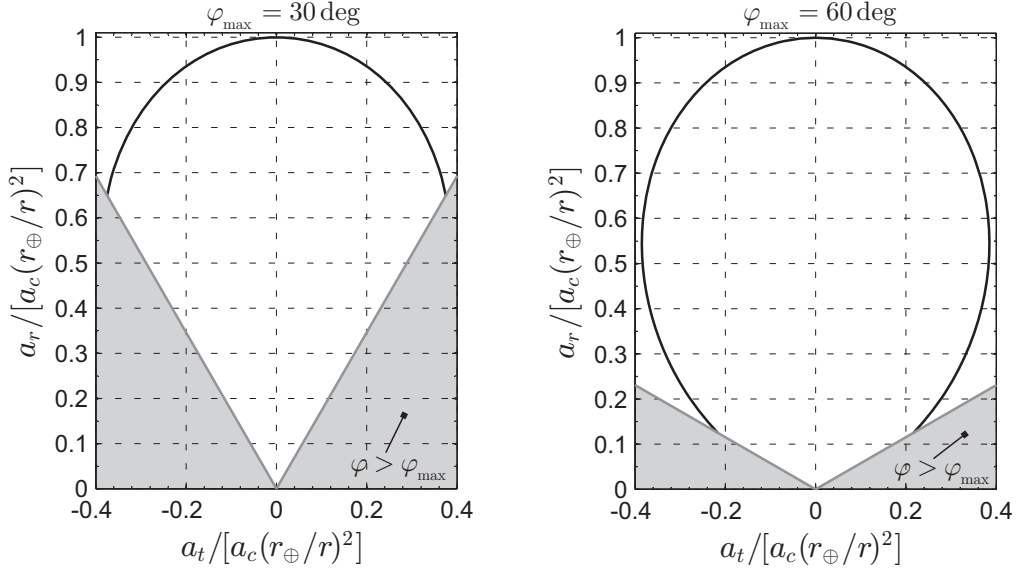Figure 4: Conceptual scheme of IKAROS spacecraft and Sun angle φ of solar panels.

Figure 5: Shape of the ideal sail force bubble as a function of $\varphi_{\max} = \{30, 60\}$ deg.

$\varphi_{\max}$ limits the maximum admissible value of the sail cone angle. The effects of $\varphi_{\max}$ on the solar sail performance are quantified in two typical mission cases, that is, an Earth-Mars and an Earth-Venus interplanetary transfer, as is discussed in the next section. In particular, the constrained trajectory optimization has been conducted by adapting the mathematical model discussed in Ref. [37] with the introduction of the additional constraint given by Eq. (9).

3. Case Study and Simulation Results

Consider a simplified Earth-Mars and Earth-Venus interplanetary transfer in which the heliocentric orbits of Earth, Mars, and Venus are all coplanar and circular with radius $r_{\oplus} \triangleq 1$ au, $r_{\sigma} \triangleq 1.523$ au , and $r_{\female} \triangleq 0.723$ au, respectively. Assume all planetary orbits to belong to the (x, y) plane of the inertial reference

frame $\mathcal{T}$; see Fig. 1. In such a two-dimensional case, the y_O-axis of the orbital frame coincides with the z-axis of the inertial frame, that is, $\hat{\boldsymbol{j}}_O = \hat{\boldsymbol{k}}$; see Fig. 2(a). Therefore, the normal unit vector $\hat{\boldsymbol{n}}$ belongs to the (x, y) plane and the sail clock angle assumes two values only, either $\delta = 0$ or $\delta = 180\,\text{deg}$. As a result, the solar sail attitude can be described by a single auxiliary control angle α_a defined as

$$\alpha_a \triangleq \text{sign}\,(\cos\delta)\,\alpha \tag{10}$$

where $\text{sign}\,(\square) \in \{-1,\,1\}$ is the signum function. Three different values of characteristic acceleration are used in the simulations, that is, $a_c = \{0.1,\,1,\,2\}\,\text{mm/s}^2$, which are representative of a low-performance ($a_c = 0.1\,\text{mm/s}^2$), a medium-performance ($a_c = 1\,\text{mm/s}^2$), and a high-performance ($a_c = 2\,\text{mm/s}^2$) solar sail. The unconstrained minimum flight times Δt_u for an ideal flat sail, that is, the minimum transfer times obtained when $\varphi_{\max} = 90\,\text{deg}$, are reported in Tab. 1, while the (dimensionless) time variation of the optimal control law $\alpha_a = \alpha_a(t)$ is drawn in Fig. 6. Finally, Fig. 7 shows the polar plots of the optimal transfer trajectories in the two mission scenarios.

| $a_c\,[\text{mm/s}^2]$	target planet	
	Mars	Venus
0.1	2661.5	1161.3
1	407.7	204.7
2	323.9	163.6

Table 1: Minimum flight time Δt_u [days] for a coplanar, circle-to-circle, interplanetary transfer without solar panel angle constraints.

When the additional constraint on $\varphi_{\max}$ is included in the trajectory optimization, the minimum flight time becomes larger than the value of Δt_u reported in Tab. 1. More precisely, Fig. 8 shows the curve levels of the dimensionless minimum flight times $\Delta t = \Delta t(a_c, \varphi_{\max})$ for the two mission scenarios when the maximum value of φ is varied in the range $\varphi_{\max} \in [30, 90]\,\text{deg}$.

Figure 8 clearly shows that the constraint on the maximum value of the cone angle has a substantial impact on the time of flight, especially in the case of a high performance solar sail and a small value of $\varphi_{\max}$. For example, when $a_c = 2\,\text{mm/s}^2$ and $\varphi_{\max} = 30\,\text{deg}$, the flight time of an Earth-Venus (or Earth-Mars) transfer is about 225 days (or 431 days), which corresponds to an increment of 38% (or 33%) with respect to the unconstrained case Δt_u; see Tab. 1. In particular, for a fixed value of the characteristic acceleration, the function $\Delta t = \Delta t(\varphi_{\max})$ shows a similar trend for both the mission cases in the investigated range of angle $\varphi_{\max}$.

An interesting feature can be observed in Fig. 8, which shows that beyond a certain value of $\varphi_{\max}$, the time of flight Δt tends to the value Δt_u of the unconstrained scenario. This behaviour can be simply explained by observing that, for some values of a_c, the optimal control law $\alpha_a = \alpha_a(t)$ for the unconstrained case has a maximum value lower than $90\,\text{deg}$, that is, $\alpha_a^{\max} \triangleq \max(|\alpha_a|) \leq 90\,\text{deg}$; see Figs. 6(a) and 6(b). In particular, the variation of $\alpha_a^{\max}$ with a_c is drawn in Fig. 9 for an unconstrained scenario. Note that $\alpha_a^{\max} = 90\,\text{deg}$ only when the characteristic acceleration is beyond the canonical value of $1\,\text{mm/s}^2$. In other terms, Fig. 9 shows that a coasting arc (i.e. a phase in which the sail is oriented edgewise to the Sun) appears in the optimal transfer trajectory towards Mars or Venus when a medium-high performance solar sail is considered [38]. For example, when $a_c = 0.1\,\text{mm/s}^2$, $\alpha_a^{\max} \simeq 37.3\,\text{deg}$ (or $\alpha_a^{\max} \simeq 38.5\,\text{deg}$) for an Earth-Venus (or an Earth-Mars) transfer. This behaviour is consistent with the results of Ref. [26], which reports the solar sail optimal flight times, obtained in closed form with a semi-analytical model, corresponding to a heliocentric orbit raising (or lowering) case. In fact, the value of $\alpha_a^{\max} \simeq 37.3\,\text{deg}$ (or $\alpha_a^{\max} \simeq 38.5\,\text{deg}$) is close to $\widetilde{\alpha}_a \triangleq \arcsin(\sqrt{3}/3) \simeq 35.2\,\text{deg}$, for which the component of propulsive acceleration in the transverse direction is maximized. Therefore, if $\varphi_{\max} \geq \alpha_a^{\max}$, the constraint on $\varphi_{\max}$ is always inactive, and the results of the optimization process for the constrained and unconstrained cases coincide.

When $\alpha_a^{\max} > \varphi_{\max}$, the constraint on $\varphi_{\max}$ significantly affects the optimal control law. For example assume $\varphi_{\max} = 45\,\text{deg}$, as in the case of IKAROS mission [39]. If the characteristic acceleration is chosen to be $a_c = 1\,\text{mm/s}^2$, the optimal control law for both cases is shown in Fig. 10. The latter is much different from that computed in the unconstrained case; compare Figs. 10(a) and 10(b) with Figs. 6(c) and 6(d),
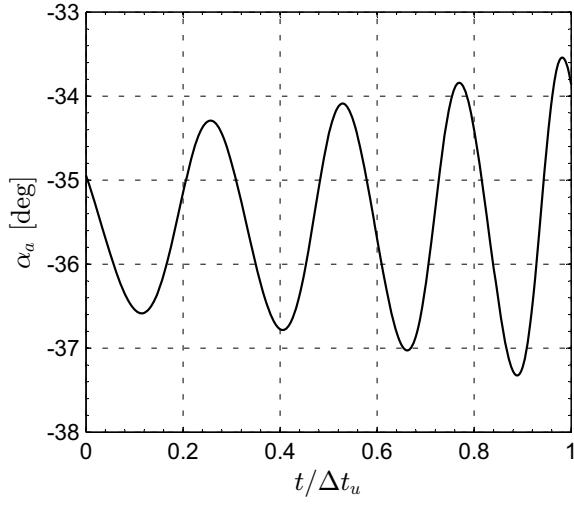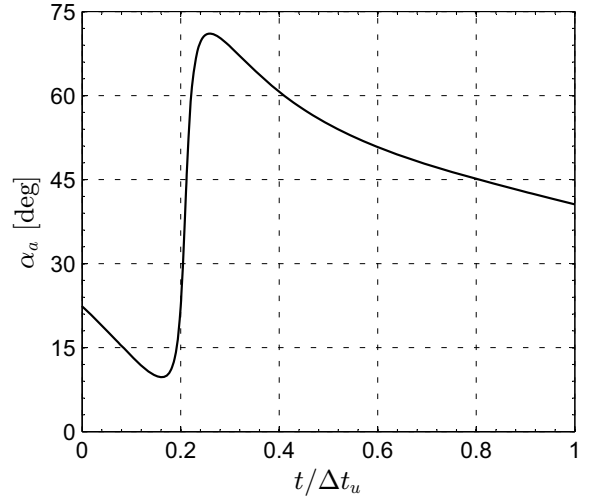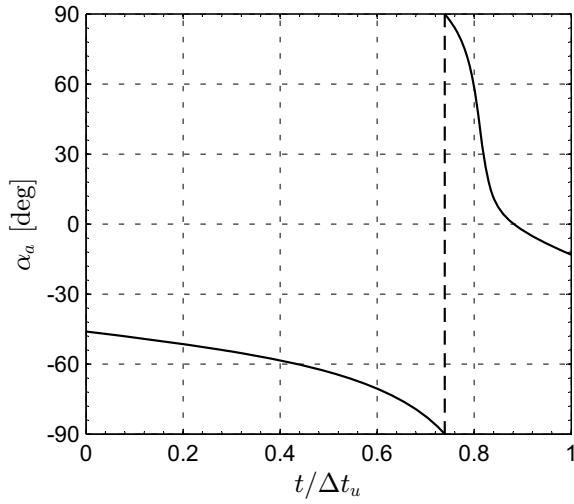
(a) Earth-Venus, $a_c = 0.1\,\mathrm{mm/s^2}$.
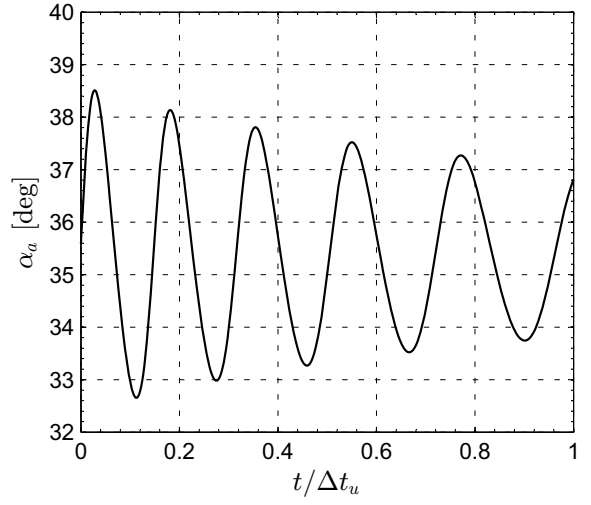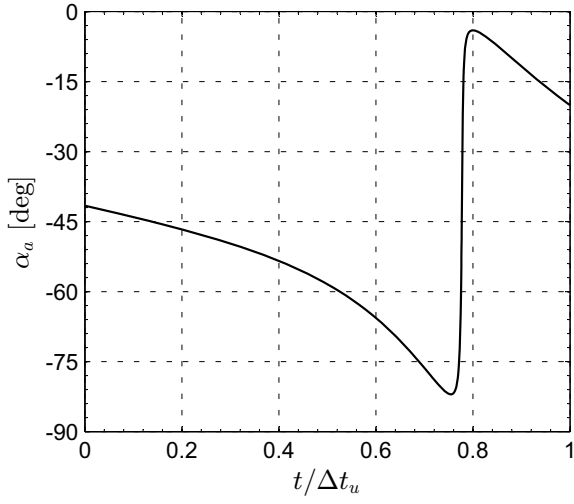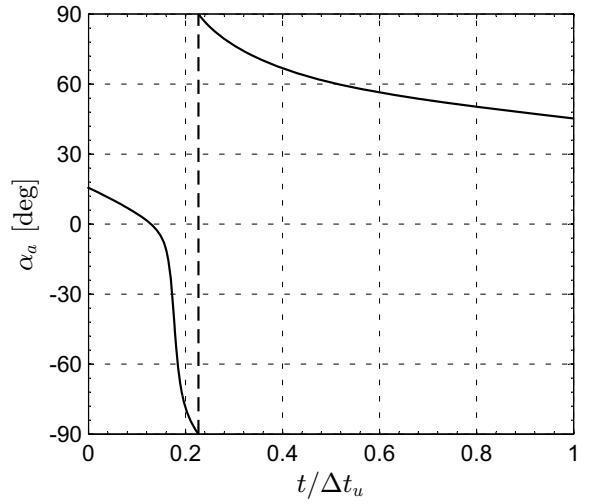
(b) Earth-Mars, $a_c = 0.1\,\mathrm{mm/s^2}$.

(c) Earth-Venus, $a_c = 1\,\mathrm{mm/s^2}$.
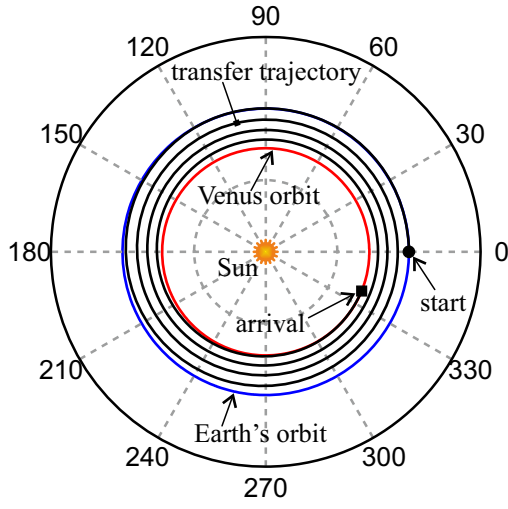
(d) Earth-Mars, $a_c = 1\,\mathrm{mm/s^2}$.

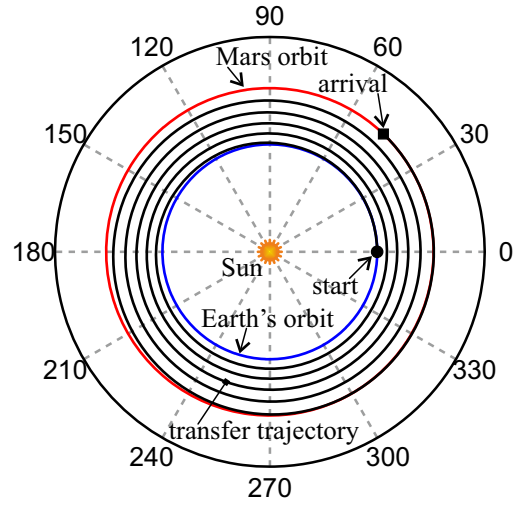(e) Earth-Venus, $a_c = 2\,\mathrm{mm/s^2}$.

(f) Earth-Mars, $a_c = 2\,\mathrm{mm/s^2}$.

Figure 6: Optimal control law for an unconstrained (i.e., $\varphi_{\max} = 90\,\mathrm{deg}$) interplanetary transfer.
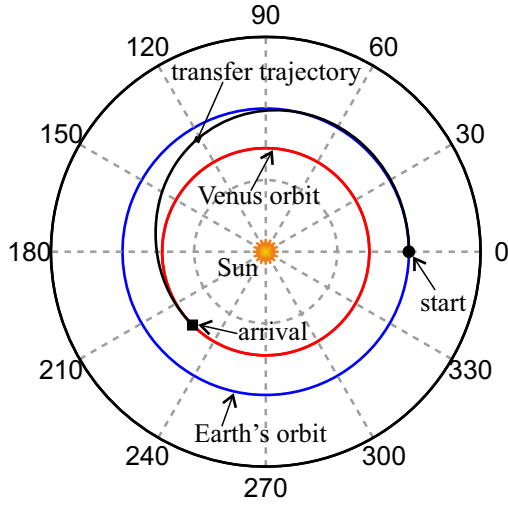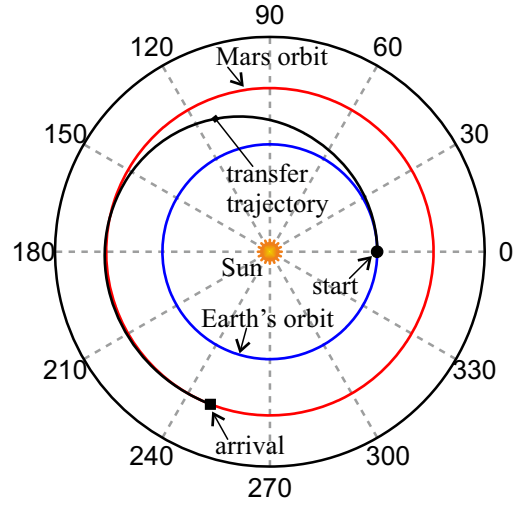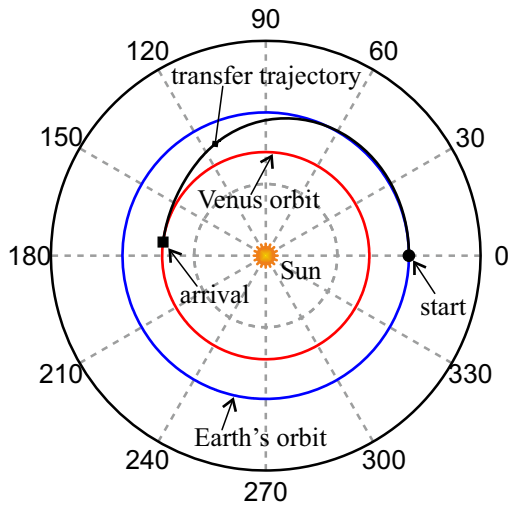
(a) Earth-Venus, $a_c = 0.1\,\mathrm{mm/s^2}$.

(b) Earth-Mars, $a_c = 0.1\,\mathrm{mm/s^2}$.

(c) Earth-Venus, $a_c = 1\,\mathrm{mm/s^2}$.

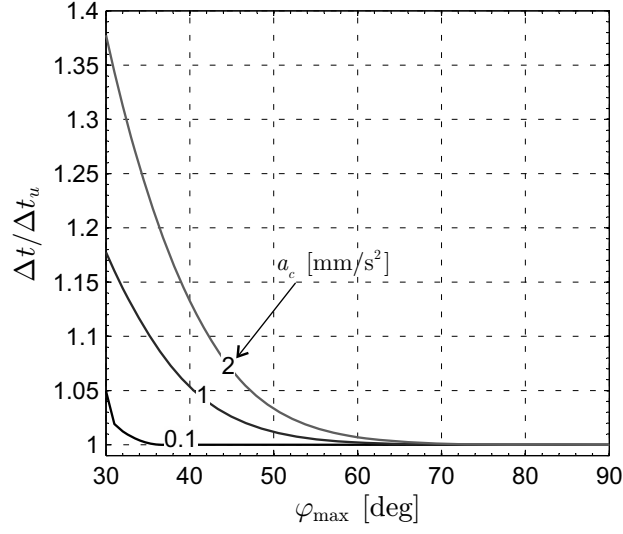(d) Earth-Mars, $a_c = 1\,\mathrm{mm/s^2}$.
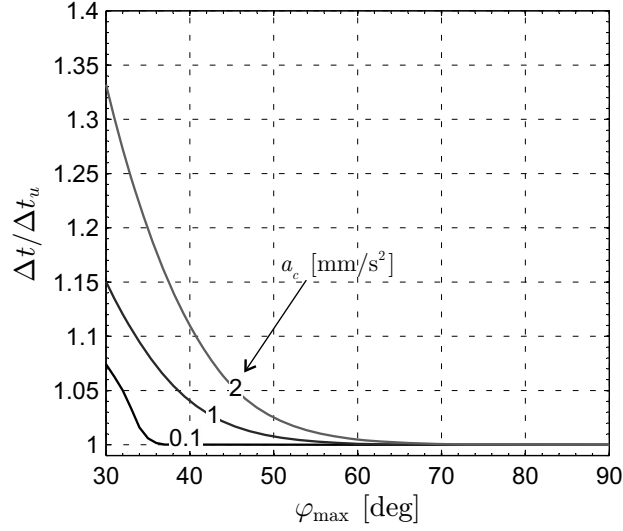
(e) Earth-Venus, $a_c = 2\,\mathrm{mm/s^2}$.
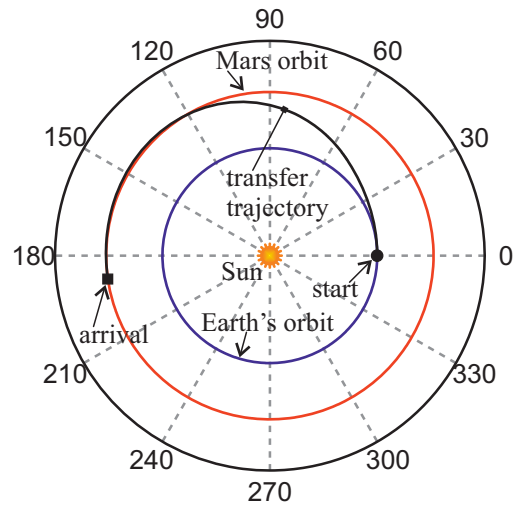
(f) Earth-Mars, $a_c = 2\,\mathrm{mm/s^2}$.

Figure 7: Optimal trajectory for an unconstrained (i.e., $\varphi_{\max} = 90\,\mathrm{deg}$) interplanetary transfer.

9

(a) Earth-Venus transfer.

(b) Earth-Mars transfer.

Figure 8: Minimum (dimensionless) flight time Δt for a coplanar, circle-to-circle, constrained interplanetary transfer as a function of $\varphi_{\max}$.

respectively. From the numerical simulations, a very small increment of the time of flight is observed with respect to the unconstrained case, with a difference of 3% (or 2%) of Δt_u for the Earth-Venus (or Earth-Mars) scenario; see Fig. 8.

In fact, for the chosen values of $\{a_c, \varphi_{\max}\}$, the transfer trajectories in the constrained case are very similar to those obtained in the unconstrained scenario, as can be deduced by comparing Figs. 11(a) and 11(b) with 7(c) and 7(d), respectively. In particular, Fig. 11 shows the interval within which the cone angle-constraint is active during the interplanetary transfer (grey tick line in the trajectory polar curve). The differences between constrained and unconstrained case may be appreciated with the aid of Fig. 12, which shows the time-variation of the spacecraft state variables, i.e., the Sun-spacecraft distance r, and the radial and transverse components of the spacecraft velocity (u and v, respectively).
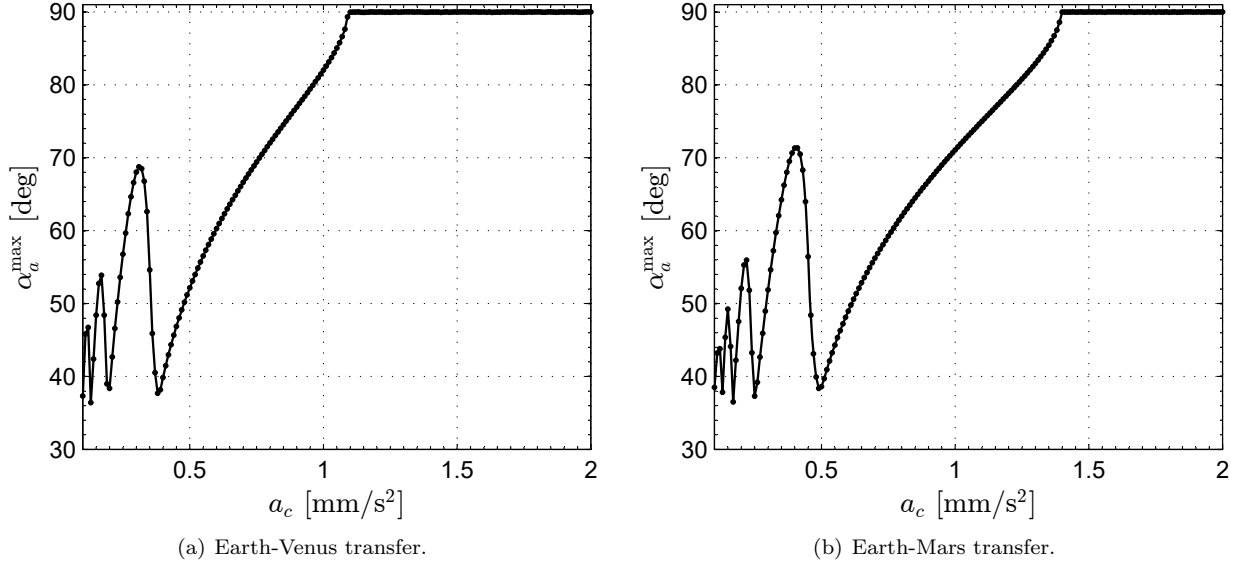
(a) Earth-Venus transfer.

(b) Earth-Mars transfer.

Figure 9: Variation of $\alpha_a^{\max}$ with a_c for an unconstrained (i.e., $\varphi_{\max} = 90\,\mathrm{deg}$) scenario.

(a) Earth-Venus transfer.

(b) Earth-Mars transfer.
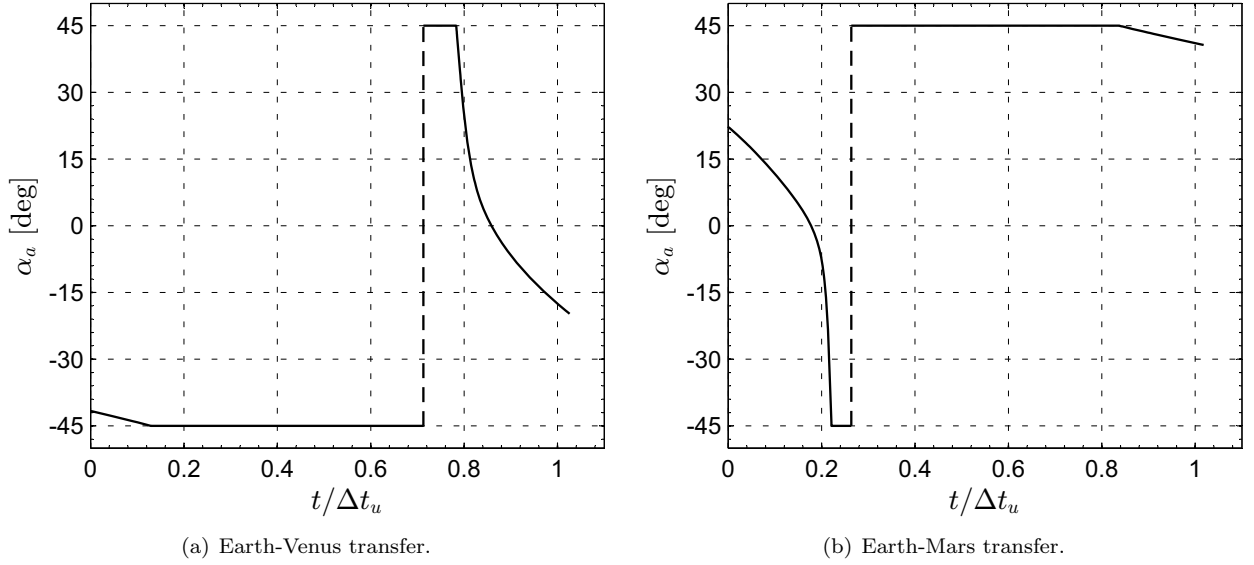
Figure 10: Optimal control law when $a_c = 1\,\mathrm{mm/s^2}$ and $\varphi_{\max} = 45\,\mathrm{deg}$.

4. Conclusions

This paper has analyzed the effect of an additional constraint on the maximum value of the cone angle on the performance of an ideal solar sail in a two-dimensional, circle-to-circle, interplanetary transfer. The numerical simulations have shown that the minimum time of flight increases significantly with respect to the unconstrained reference case when a high performance solar sail (that is, with a high value of characteristic acceleration) is considered, and the maximum admissible value of the cone angle is sufficiently low. Moreover, the constraint on the maximum value of the cone angle implies a pronounced variation in the optimal control law, even if the flight time and the optimal trajectory are very close to those of the reference unconstrained case. Similar results are also to be expected in three-dimensional interplanetary transfers, or when dealing with non-ideal solar sails. Those investigations are left to future research.
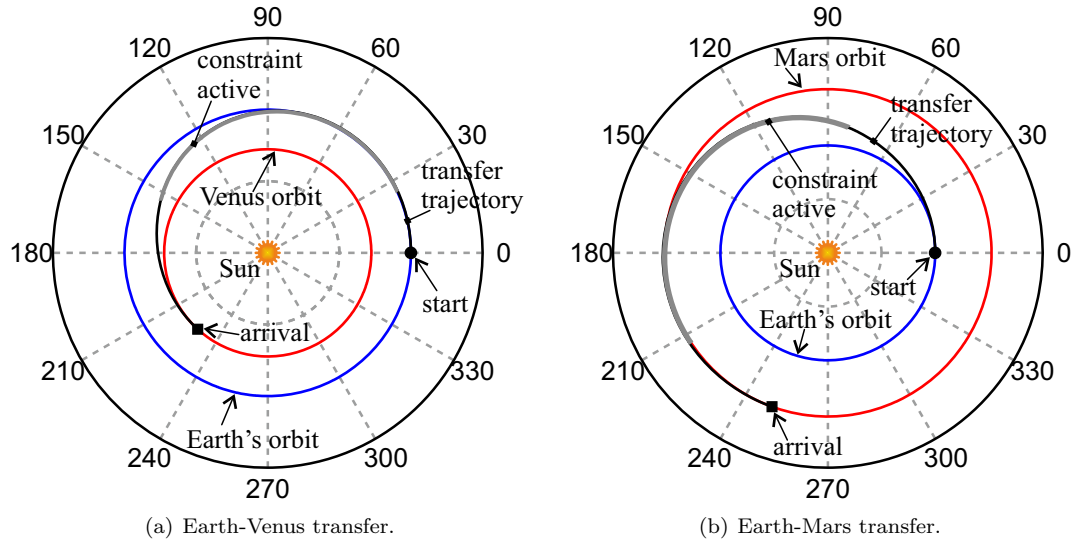
11

(a) Earth-Venus transfer.

(b) Earth-Mars transfer.

Figure 11: Optimal transfer trajectory when $a_c = 1 \, \text{mm/s}^2$ and $\varphi_{\max} = 45 \, \text{deg}$.

References

[1] B. Fu, E. Sperber, F. Eke, Solar sail technology–a state of the art review, Progress in Aerospace Sciences 86 (2016) 1–19, doi: 10.1016/j.paerosci.2016.07.001.

[2] S. Gong, M. Macdonald, Review on solar sail technology, Astrodynamics 3 (2019) 93–125, doi: 10.1007/s42064-019-0038-x.

[3] J. L. Wright, Space Sailing, Gordon and Breach Science Publishers , 1992, pp. 223–233.

[4] B. Dachwald, et al., Potential solar sail degradation effects on trajectory and attitude control, in: AIAA Guidance, Navigation, and Control Conference and Exhibit, San Francisco, USA, 2005, paper AIAA 2005-6172.

[5] B. Dachwald, G. Mengali, A. A. Quarta, M. Macdonald, Parametric model and optimal control of solar sails with optical degradation, Journal of Guidance, Control, and Dynamics 29 (5) (2006) 1170–1178, doi: 10.2514/1.20313.

[6] B. Dachwald, M. Macdonald, C. R. McInnes, G. Mengali, A. A. Quarta, Impact of optical degradation on solar sail mission performance, Journal of Spacecraft and Rockets 44 (4) (2007) 740–749, doi: 10.2514/1.21432.

[7] E. E. Montgomery, G. P. Garbe, A. F. Heaton, Places only solar sails can go, in: AIAA International Air and Space Symposium and Exposition: The Next 100 Years, Dayton, USA, 2003, paper AIAA 2003-2836.

[8] M. Macdonald, C. R. McInnes, Solar sail science mission applications and advancement, Advances in Space Research 48 (11) (2011) 1702–1716, doi: 10.1016/j.asr.2011.03.018.

[9] X. Zeng, K. T. Alfriend, S. R. Vadali, Solar sail planar multireversal periodic orbits, Journal of Guidance, Control, and Dynamics 37 (2) (2014) 674–681, doi: 10.2514/1.58598.

[10] X. Zeng, G. Vulpetti, C. Circi, Solar sail h-reversal trajectory: A review of its advances and applications, Astrodynamics 3 (1) (2019) 1–15, doi: 10.1007/s42064-018-0032-y.

[11] E. Ancona, R. Y. Kezerashvili, G. L. Matloff, Exploring the kuiper belt with sun-diving solar sails, Acta Astronautica 160 (2019) 601–605, doi: 10.1016/j.actaastro.2019.02.019.

[12] Y. Song, S. Gong, Solar sail trajectory optimization of multi-asteroid rendezvous mission, Acta Astronautica 157 (2019) 111–122, doi: 10.1016/j.actaastro.2018.12.016.

[13] S. Kikuchi, J. Kawaguchi, Asteroid de-spin and deflection strategy using a solar-sail spacecraft with reflectivity control devices, Acta Astronautica 156 (2019) 375–386, doi: 10.1016/j.actaastro.2018.06.047.

[14] P. Kelly, R. Bevilacqua, An optimized analytical solution for geostationary debris removal using solar sails, Acta Astronautica 162 (2019) 72–86, doi: 10.1016/j.actaastro.2019.05.055.

[15] R. L. Garwin, Solar sailing: A practical method of propulsion within the solar system, Jet Propulsion 28 (123) (1958) 188–190, doi: 10.2514/8.7271.

[16] T. C. Tsu, Interplanetary travel by solar sail, ARS Journal 29 (6) (1959) 422–427, doi: 10.2514/8.4791.

[17] L. Johnson, Solar sail propulsion for interplanetary small spacecraft, in: Space Propulsion 2018, Seville, Spain, 2018, paper SP2018-00017.

[18] C. G. Sauer, Optimum solar-sail interplanetary trajectories, in: AIAA/AAS Astrodynamics Conference, San Diego (CA), 1976.

[19] B. Dachwald, Minimum transfer times for nonperfectly reflecting solar sailcraft, Journal of Spacecraft and Rockets 41 (4) (2004) 693–695, doi: 10.2514/1.6279.

[20] X. Zeng, S. Gong, J. Li, Fast solar sail rendezvous mission to near earth asteroids, Acta Astronautica 105 (1) (2014) 40–56, doi: 10.1016/j.actaastro.2014.08.023.

[21] C. R. McInnes, Solar Sailing: Technology, Dynamics and Mission Applications, Springer-Praxis Series in Space Science and Technology, Springer-Verlag, Berlin, 1999, Ch. 5.
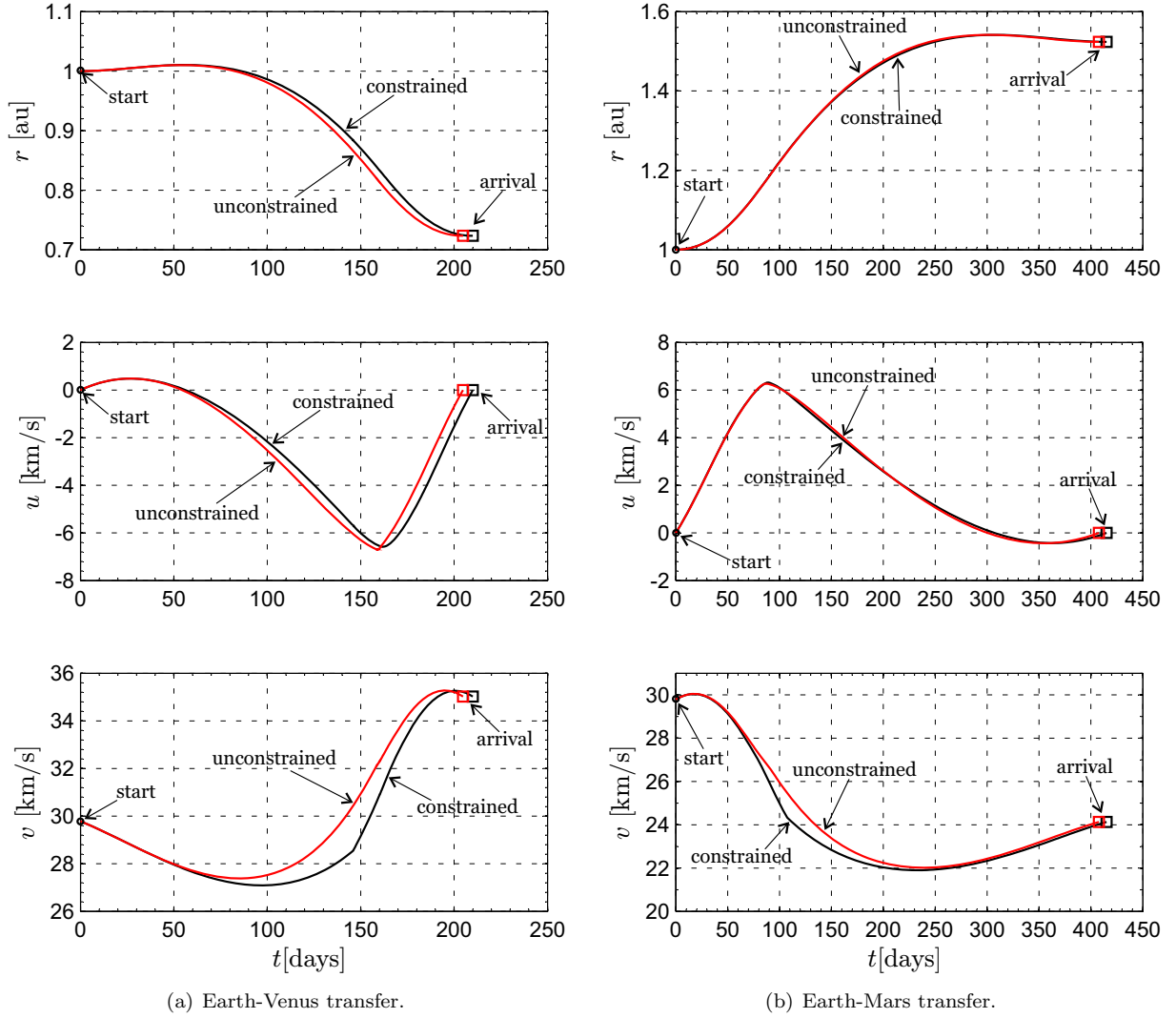
12

(a) Earth-Venus transfer.

(b) Earth-Mars transfer.

Figure 12: Time-variation of the spacecraft state variables when $a_c = 1\,\mathrm{mm/s^2}$ and $\varphi_{\mathrm{max}} = 45\,\mathrm{deg}$: constrained vs. unconstrained scenario.

[22] B. Wie, Thrust vector control analysis and design for solar-sail spacecraft, Journal of Spacecraft and Rockets 44 (3) (2007) 545–557, doi: 10.2514/1.23084.

[23] Y. Tsuda, O. Mori, R. Funase, H. Sawada, T. Yamamoto, T. Saiki, T. Endo, J. Kawaguchi, Flight status of IKAROS deep space solar sail demonstrator, Acta Astronautica 69 (9-10) (2011) 833–840, doi: 10.1016/j.actaastro.2011.06.005.

[24] L. Johnson, M. Whorton, A. Heaton, R. Pinson, G. Laue, C. Adams, NanoSail-D: A solar sail demonstration mission, Acta Astronautica 68 (5-6) (2011) 571–575, doi: 10.1016/j.actaastro.2010.02.008.

[25] J. He, S.-P. Gong, F.-H. Jiang, J.-F. Li, Time-optimal rendezvous transfer trajectory for restricted cone-angle range solar sails, Acta Mechanica Sinica 30 (5) (2014) 628–635, doi: 10.1007/s10409-014-0033-x.

[26] A. A. Quarta, G. Mengali, Semi-analytical method for the analysis of solar sail heliocentric orbit raising, Journal of Guidance, Control, and Dynamics 35 (1) (2012) 330–335, doi: 10.2514/1.55101.

[27] A. Caruso, A. A. Quarta, G. Mengali, Comparison between direct and indirect approach to solar sail circle-to-circle orbit raising optimization, Astrodynamics 3 (3) (2019) 273–284, doi: 10.1007/s42064-019-0040-x.

[28] L. Boni, G. Mengali, A. A. Quarta, Solar sail structural analysis via improved finite element modeling, Proceedings of the Institution of Mechanical Engineers, Part G: Journal of Aerospace Engineering 231 (2) (2017) 306–318, doi: 10.1177/0954410016636164.

[29] L. Boni, A. A. Quarta, G. Mengali, Thermal-structural analysis of a square solar sail, Acta Astronautica 154 (2019) 268–277, doi: 10.1016/j.actaastro.2018.03.037.

[30] L. Boni, G. Mengali, A. A. Quarta, Finite element analysis of solar sail force model with mission application, Proceedings of the Institution of Mechanical Engineers, Part G: Journal of Aerospace Engineering 233 (5) (2019) 1838–1846, doi: 10.1177/0954410018764183.

[31] G. Vulpetti, Sailcraft at high speed by orbital angular momentum reversal, Acta Astronautica 40 (10) (1997) 733–758, doi: 10.1016/S0094-5765(97)00153-7.

[32] A. A. Quarta, G. Mengali, Solar sail capabilities to reach elliptic rectilinear orbits, Journal of Guidance, Control, and Dynamics 34 (3) (2011) 923–926, doi: 10.2514/1.51638.

[33] A. A. Quarta, G. Mengali, Optimal solar sail transfer to linear trajectories, Acta Astronautica 82 (2) (2013) 189–196, doi: 10.1016/j.actaastro.2012.03.005.

[34] X. Zeng, K. T. Alfriend, J. Li, S. R. Vadali, Optimal solar sail trajectory analysis for interstellar missions, in: 22nd AAS/AIAA Space Flight Mechanics Meeting, Vol. 143, Charleston, SC (United States), 2012, pp. 1951–1964.

[35] G. Mengali, A. A. Quarta, C. Circi, B. Dachwald, Refined solar sail force model with mission application, Journal of Guidance, Control, and Dynamics 30 (2) (2007) 512–520, doi: 10.2514/1.24779.

[36] L. Niccolai, M. Bassetto, A. A. Quarta, G. Mengali, A review of smart dust architecture, dynamics, and mission applications, Progress in Aerospace Sciences 106 (2019) 1–14, doi: 10.1016/j.paerosci.2019.01.003.

[37] G. Mengali, A. A. Quarta, Rapid solar sail rendezvous missions to asteroid 99942 apophis, Journal of Spacecraft and Rockets 46 (1) (2009) 134–140, doi: 10.2514/1.37141.

[38] C. G. Sauer, A comparison of solar sail and ion drive trajectories for a halley's comet rendezvous mission, in: AAS/AIAA Astrodynamics Conference, Jackson Hole, WY; US, 1977, AAS paper 77-4.

[39] O. Mori, H. Sawada, R. Funase, T. Endo, M. Morimoto, T. Yamamoto, Y. Tsuda, Y. Kawakatsu, J. Kawaguchi, Development of first solar power sail demonstrator - IKAROS, in: Proceedings of 21st International Symposium on Space Flight Dynamics (ISSFD), Toulouse, France, 2009.